Toxicon 204 (2021) 44–55

Contents lists available at ScienceDirect

Toxicon

journal homepage: www.elsevier.com/locate/toxicon

The pore-forming activity of sticholysin I is enhanced by the presence of a phospholipid hydroperoxide in membrane

Maressa Donato [a,b], Carmen Soto [c], María Eliana Lanio [c], Rosangela Itri [a,**], Carlos Álvarez [c,*]

[a] Instituto de Física, Universidade de São Paulo (USP), São Paulo, SP, Brazil
[b] Center for Laser and Applications, Nuclear and Energy Research Institute, São Paulo, Brazil
[c] Centro de Estudio de Proteínas, Facultad de Biología, Universidad de La Habana, CP, 10400, La Habana, Cuba

ARTICLE INFO

Handling Editor: Ray Norton

Keywords:
Actinoporins
Pore-forming toxins
Membrane permeabilization
Membrane fluidity
Phase-coexistence
1-Palmitoyl 2-oleoylphosphatidylcholine hydroperoxide

ABSTRACT

Sticholysin I (StI) is a pore-forming toxin (PFT) belonging to the actinoporin protein family characterized by high permeabilizing activity in membranes. StI readily associates with sphingomyelin (SM)-containing membranes originating pores that can lead to cell death. Binding and pore-formation are critically dependent on the physicochemical properties of membrane. 1-palmitoyl-2-oleoylphosphatidylcholine hydroperoxide (POPC–OOH) is an oxidized phospholipid (OxPL) containing an –OOH moiety in the unsaturated hydrocarbon chain which orientates towards the bilayer interface. This orientation causes an increase in the lipid molecular area, lateral expansion and decrease in bilayer thickness, elastic and bending modulus, as well as modification of lipid packing. Taking advantage of membrane structural changes promoted by POPC-OOH, we investigated its influence on the permeabilizing ability of StI. Here we report the action of StI on Giant Unilamellar Vesicles (GUVs) made of 1-palmitoyl-2-oleoylphosphatidylcholine (POPC) and SM containing increasing amount of POPC-OOH to assess vesicle permeability changes when compared to OxPL-lacking membranes. Inclusion of POPC-OOH in membranes did not promote spontaneous vesicle leaking but resulted in increased membrane permeability due to StI action. StI activity did not modify the fluid-gel phase coexistence boundaries neither in POPC:SM or POPC-OOH:SM membranes. However, the StI insertion mechanism in membrane seems to differ between POPC:SM and POPC-OOH:SM mixtures as suggested by changes in the time course of monolayer surface tension measurements, even though a preferable binding of the toxin to OxPL-containing systems could not be here demonstrated. In summary, modifications in the membrane imposed by lipid hydroperoxidation favor StI permeabilizing activity.

1. Introduction

Sea anemones (Actiniaria) produce a vast family of cytolytic polypeptides to attack or self-defend (Anderluh and Lakey, 2008; Anderluh and Macek, 2002). The term actinoporin was coined to designate one of these families, which comprises mainly monomeric, soluble, α-helical Pore Forming Toxins (PFTs) with a molecular mass of around 20 kDa, the majority with a basic pI (>9.0), lacking Cys residues, and a high affinity for sphingomyelin (SM) - containing membranes. They were discovered as lethal hemolysins or cytolysins and inhibited by SM (Kem, 1988). Actinoporins are well known by their high cytolytic/permeabilizing activity in the low nanomolar concentration range, both in cells and model membranes (Álvarez et al., 2009; Ros et al., 2015).

Sticholysin I (StI) is one of the actinoporins synthesized by the sea anemone *Stichodactyla helianthus*. The overall structure of StI, as well as that of other actinoporins, is characterized by a stiff central core formed by two β-sheets and by two α-helices arranged perpendicularly to each other on both sides of the central core. The α-helix located closest to the N-terminal helix is amphipathic, mobile, and flexible and is involved in pore-formation (García-Linares et al., 2013; Mancheño et al., 2003) (Fig. 1A).

Abbreviations: EqtII, equinatoxin II; FraC, fragaceatoxin C; GUVs, giant unilamellar vesicles; LUVs, large unilamellar vesicles; Ld, liquid disordered phase; Lo, liquid ordered phase; OxPL, oxidized phospholipid; PC, phosphatidylcholine; POPC, 1-palmitoyl-2-oleoylphosphatidylcholine; POPC-OOH, the hydroperoxidized form of POPC; PFT, pore-forming toxin; SM, sphingomyelin; So, gel phase/solid ordered phase; StI, sticholysin I; SUVs, small unilamellar vesicles.

* Corresponding author.
** Corresponding author. Departamento de Física Aplicada, Instituto de Física, Universidade de São Paulo (USP), Brazil.
E-mail addresses: itri@if.usp.br (R. Itri), calvarez@fbio.uh.cu (C. Álvarez).

https://doi.org/10.1016/j.toxicon.2021.10.012
Received 6 September 2021; Received in revised form 23 October 2021; Accepted 29 October 2021
Available online 1 November 2021

The essential and specific role of SM in the interaction of sticholysins (Sts) with membranes has been well documented. In their early work, Bernheimer and Avigad (1976) purified the S. helianthus toxin originally reported by Devlin (1974) and demonstrated that the hemolytic activity was specifically inhibited by SM proposing that this sphingophospholipid could function as its receptor in the red blood cell membrane (Bernheimer and Avigad, 1976; Linder et al., 1977). The presence of SM domains in the bilayer provided optimal conditions for insertion into the membrane and subsequent assembly of a stable multimeric complex which functions as an ion channel (Doyle et al., 1989).

The mechanism of pore formation by actinoporins in membranes is a several stage process consisting in: (i). membrane binding, (ii). oligomerization, detachment and insertion of the N-terminus into the hydrophobic nucleus of the membrane, and (iii). pore assembly. The binding of the protomers to the membrane through the aromatic residues and lipid-binding sites was identified as the first stage in this sequence. Upon binding to the membrane, the concomitant association of several AP monomers and the relocation of the N-terminus from the toxin body to the hydrophobic nucleus of the bilayer takes place (García-Linares et al., 2013; Hong et al., 2002; Malovrh et al., 2003; Mancheño et al., 2003; Rojko et al., 2016).

StI readily associates with SM-containing membranes originating pores that eventually can lead to cell death (Tejuca et al., 1996; Valcarcel et al., 2001). These are cation-selective pores of 2 nm in diameter, both in model and cell membranes, leading to cell death by osmotic shock (Tejuca et al., 1996, 2001). It has been extensively reported that SM is a basic constituent for actinoporin effective membrane binding resulting in pore formation (Bakrac and Anderluh, 2010; Tejuca et al., 1996; Valcarcel et al., 2001). Experimental evidence indicates that actinoporins recognize SM through both its polar head group and ceramide unit (Maula et al., 2013; Soto et al., 2017); of relevance, SM ensures irreversible binding and pore generation in model membranes (Martínez et al., 2007; Michaels, 1979; Valcarcel et al., 2001). The association of Sts to membranes leading to pore formation responds significantly to the nature of lipid head groups and particularly to their access to the SM interfacial structural motif (Soto et al., 2017).

The mechanism of pore formation due to APs binding to the membrane is still a matter of debate. Previous work proposed that the membrane affinity of actinoporins is dependent on the SM presence but only if the membrane exhibits phase coexistence (Schön et al., 2008), whereas other has postulated that this activity occurs even in those lipid systems lacking SM provided they exhibit phase separation (Barlic et al., 2004). In the case of Sts, rather than the sole presence of the lipid platforms, our previous studies revealed that binding of Sts to membranes is the result of a fine tune between SM concentration and membrane fluidity (Pedrera et al., 2014, 2015). Therefore, since the membrane has an adequate availability of SM, physical properties of the lipid ensemble, such as its phase state and rheological properties, become a leading character in its recognition by Sts. Consistent with this, we advanced the hypothesis that a fluid phase with a looser lipid packing in respect to a gel phase and a scenario favoring StI-sphingolipid interaction by H-bonds provide a favorable platform for competent toxin association (Pedrera et al., 2014).

Regardless of these considerations, the modulation of actinoporin activity due to the existence of lateral phase separation in membrane is still an unresolved issue. In this direction, it has been claimed that actinoporin EqtII association to lipids is favored by the presence of packing defects on the membrane surface (Alegre-Cebollada et al., 2006; Barlic et al., 2004; Schön et al., 2008). On the other hand, the simultaneous presence of SM and Chol in membrane significantly favors binding and pore formation by Sts (Martínez et al., 2007) and EqtII (Drechsler et al., 2010). Our studies on liposomes and lipid monolayers demonstrated that ternary lipid systems in which Chol, ergosterol or cholestenone were mixed with phosphatidylcholine (PC) and SM favor binding, insertion, and pore formation by StI. Interestingly, the enhancement of StI activity in membranes containing any of the three sterols occurs irrespectively of their ability to promote lateral phase separation (Pedrera et al., 2015). We then speculated that sterols promote changes in the membranes properties as a result of increased molecular heterogeneity, modulation of fluidity and/or induction of membrane negative curvature that impacted StI activity (Pedrera et al., 2015).

Lipids containing functionalized and truncated acyl chains are known to modify bulk membrane properties such as permeability, fluidity, thickness and phase segregation (Haluska et al., 2012; Itri et al., 2014; Sankhagowit et al., 2014; Tsubone et al., 2019). In particular, oxidized phospholipids (OxPLs) can have hydrophilic groups hanging on acyl lipid chains, which modify membrane properties. Among these species, the hydroperoxide phospholipid POPC-OOH has been experimentally and theoretically investigated in a variety of model systems due to its modulating action on membrane properties (Corvalán et al., 2020; Jurkiewicz et al., 2012; Siani et al., 2016). The hydroperoxidized unit has a more hydrophilic character than the hydrocarbon chain environment; hence, this group tends to move towards the membrane surface (Riske et al., 2009; Rosa et al., 2018; Weber et al., 2014; Wong-Ekkabut et al., 2007). This location causes an increase in lipid molecular area (Rosa et al., 2018) and membrane surface area (Weber et al., 2014; Wong-Ekkabut et al., 2007), reduction of bilayer thickness (Rosa et al., 2018), decrease in membrane elastic modulus (Weber et al., 2014) and bending rigidity (Scanavachi et al., 2021). Moreover, this OxPL

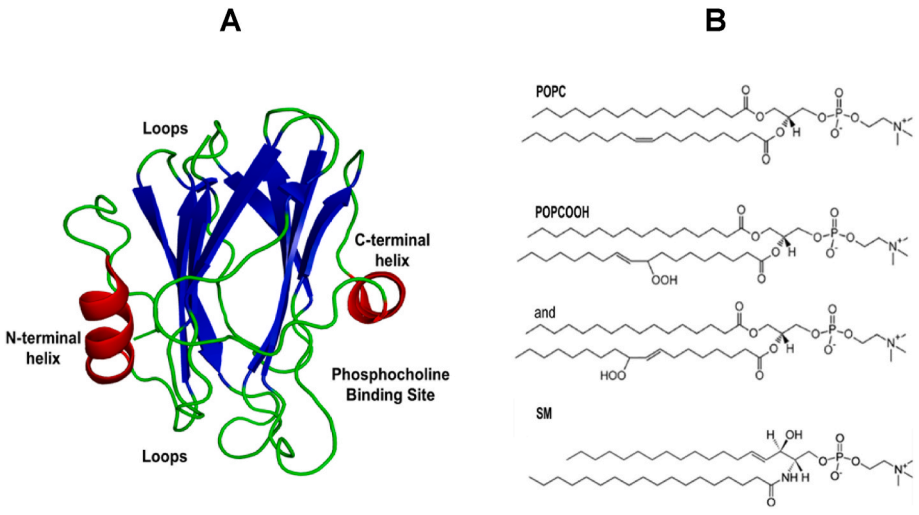

Fig. 1. Representation of StI and lipid structures. 3D ribbon representation of StI (PDB: 2KS4). 3D ribbon representation of StI (PDB: 2KS4). The 3D representation was created using Pymol 2.1. α-helices are displayed in red, β-sheets in blue, turns and loops in green. The phosphocholine (POC) binding site is also shown. The 3D representation was created using Pymol 2.1 (Schrodinger, 2018) (A). Chemical structures of 1-palmitoyl-2-oleoyl-sn-glycero-3- phosphocholine (POPC), 1-palmitoyl-2-oeloylphosphatidylcholine hydroperoxide (POPC–OOH) and sphingomyelin (SM) (B). (For interpretation of the references to colour in this figure legend, the reader is referred to the Web version of this article.)

promotes phase separation into liquid disordered (Ld)/liquid ordered (Lo) phases in dipalmitoyl phosphatidyl choline (DPPC)/1-palmitoyl-2-oleoylphosphatidylcholine (POPC)/Chol membrane systems (Tsubone et al., 2019).

To the best of our knowledge, there is no report on the action of any actinoporin on model membrane systems containing an OxPL. Therefore, we decided to investigate the impact of including a peroxidized phosphatidylcholine in membrane composition on the activity of StI, since such oxidized lipid alters significantly the polar/apolar interface of the PC membrane concomitantly with loosening packing of acyl chains (Rosa et al., 2018; Scanavachi et al., 2021; Siani et al., 2016; Wong-Ekkabut et al., 2007). This approach supported by the use of giant unilamellar vesicles, GUVs, fluorescence microscopy provides a direct observation of the influence of the OxPL on lipid microdomain landscape and its influence on StI permeabilizing activity. Here we describe for the first time the membrane permeability enhancement due to the pore-forming activity of StI on lipid systems containing the hydroperoxidized POPC combined with SM, the natural receptor (Tejuca et al., 1996; Valcarcel et al., 2001)/lipid cofactor (Tanaka et al., 2015) of actinoporins. Such finding gives a step further to better understanding the role of membrane lipid composition on actinoporin activity and can be useful to comprehend and ideally treat disorders where lipid oxidation is involved (Alvarez et al., 2020).

2. Material and methods

2.1. Chemicals and reagents

StI was purified from the sea anemone whole body homogenate by combining size exclusion chromatography on Sepahdex G-50 and cation exchange on CM-Cellulose 52 as previously described (Lanio et al., 2001). The lipids 1-palmitoyl-2-oleoyl-sn-glycero-3-phosphocholine (POPC) and brain sphingomyelin (SM) were purchased from Avanti Polar Lipids, Inc. (Alabaster, AL, USA) (Fig. 1B). POPC-OOH, the hydroperoxidized form of POPC, was obtained by irradiation of POPC as previously reported (Weber et al., 2014). In short, POPC–OOH, was obtained by irradiation of POPC in methylene blue solution. To this end, POPC was dissolved in chloroform, to which 1 mL of a 0.3 mM methanol solution of methylene blue was added. This mixture was kept in an ice bath and stirred continuously. The irradiation was performed with a tungsten lamp (500 W) for 8 h. To purify the product we used two columns, an analytical column, with smaller dimensions (150 × 4.6 mm) and a semi-preparative column (250 × 20 mm), which allowed separating a larger amount of hydroperoxide lipid. Both are ODS silica columns for reverse phase chromatography. The protocol started by using the analytical column coupled to the mass spectrometer. The product with a retention time of 7 min was POPC-OOH, with m/z 792.5. This actually represents two overlapping peaks, which are due to the isomers of the POPC-OOH (OOH group attached to either carbon 9 or carbon 10). We did not separate these isomers and all experiments were performed using this mixture (without separating the isomers). This separation is very difficult and the in situ oxidation always produces both POPC-OOH isomers. Therefore, the mixture is a better mimic of the result of a real in situ oxidation. Once characterized the chromatogram and identified the POPC-OOH peak, we made the synthesis with a larger amount of POPC and used the semi-preparative column to do the separation and then collect the POPC-OOH used in the experiments. The product that was isolated from the semi-preparative column was subsequently also checked by mass spectra (m/z 792.5). The elution condition for the analytical column was 100% methanol, 1 ml/min, and the product had a retention time of 7 min. For the semi-preparative column, the mobile phase was also 100% methanol at a flow of 10 ml/min and the product had a retention time of 12 min. The fluorescent probe L-α-phosphatidylethanolamine-N-(lissaminerhodamine B sulfonyl) ammonium salt (Rho-PE) was purchased from Avanti Polar Lipids (Alabaster, AL, USA).

2.2. Preparation of liposomal vesicles

Large Unilamellar Vesicles (LUVs). Lipids at chosen molar ratio were dissolved in chloroform:methanol 2:1 v/v and evaporated thoroughly under a N_2 flux. Multilamellar vesicles (MLVs) were obtained by hydration of the lipid film with buffer (10 mM Tris-HCl, pH 7.4), intensive vortexing and heating at temperatures over their lipid transition temperature. LUVs (~0.5 mM in buffer) with approximately 100 nm diameter were prepared by extruding a solution of MLVs as previously described (Tejuca et al., 1996).

Giant Unilamellar Vesicles. GUVs of the appropriate lipid composition (total amount: 2 mg mL^{-1} in chloroform) containing the fluorophore Rho-PE (0.2 mol%), were obtained by the electroformation technique (Angelova and Dimitrov, 1986) as previously reported (Pedrera et al., 2015). Vesicles were observed the following day at room temperature (23 ± 2 °C) to ensure that they had attained thermodynamic equilibrium phase separation.

2.3. LUVs characterization

The average size and polydispersity of the LUVs, as well as ζ potential, were measured by quasi-elastic light scattering in a Zetasizer (Nano-ZS90, Malvern, U.K.), equipped with a He–He laser of 633 nm wavelength and 4 mW (T = 22–25 °C).

2.4. Permeabilization assays

In order to perform permeabilization assays, 100 μL of electroformed GUVs were mixed with 600 μL of 0.2 M glucose solutions containing different StI concentrations (4.0–30 nM) in order to achieve diverse toxin: lipid molar ratios (~minimum 1:200). The mixture was immediately taken to the microscope chamber to carry out the continuous observations in the phase contrast mode with an inverted microscope Axiovert 200 (Carl Zeiss, Jena, Germany) equipped with a Plan Neofluar 63X Ph2 objective (NA 0.75) and A-plan 10X Ph1 (NA 0.25) objective. Osmolality adjustment of sucrose and glucose solutions to avoid differences in osmotic pressure was performed on an Osmomat 030 cryoscopic osmometer (Gonotec, Germany). The resulting GUVs preparations contained sucrose inside the vesicles and glucose in the outside milieu. This difference in the internal and external sugar solutions allowed us to observe the GUVs in phase contrast optical mode due to difference in refractive indexes. Moreover, the presence of sucrose inside vesicle made them sediment on the coverslip since sucrose has a higher molecular density, facilitating observation by the inverted microscope. Images were captured with an AxioCam HSm digital camera (Carl Zeiss, Jena, Germany). StI pore forming activity on GUVs was accounted for determining the % of GUVs that completely lost optical phase contrast in a microscope field (10× magnification) over the experimental time. In the initial condition, the total amount of non-permeabilized GUVs was taken as 0% permeabilization for that microscope field. The determination was carried out in three independent experiments. Details of the conditions used for visualizing Ld-Solid ordered (So) phase separation can be found elsewhere (Dos Santos et al., 2017).

2.5. Binding of StI to LUVs

Binding to LUVs was followed by the increase in Trp intrinsic fluorescence of StI upon vesicle addition. Protein samples, at a final concentration of 1.5 μM in 10 mM Tris-HCl pH 7.4, were excited at 295 nm in order to minimize tyrosine emission and fluorescence spectra were measured from 310 to 450 nm (Lakowicz, 2006; Martinez et al., 2001) at 23 ± 2 °C in a Steady-state spectrofluorimeter Varian, Cary-Eclipse (Agilent Technologies, Inc., Santa Clara, CA, USA). To this solution, increasing amount of LUVs of the studied composition was added up to a toxin: lipid molar ratio close to 1:200 and changes in fluorescence

intensity and λ_{max} were recorded. Control LUVs spectra were also obtained in the absence of toxin and subtracted from experimental data to correct any light scattered by vesicles.

Quenching of the fluorescence produced by Trp residues positioned in diverse microenvironments, in solution and bound to membranes under saturation conditions, was achieved through the addition of increasing amounts of acrylamide. Briefly, StI in buffer was titrated with acrylamide (0–200 mM) in the absence and presence of saturating LUVs concentrations. The ratio between StI fluorescence intensity maximum without acrylamide (F_o) and in the presence of the quencher (F) was plotted as a function of acrylamide concentration and the experimental points were analyzed by the Stern-Volmer equation:

$$F_o / F = 1 + Ksv[Q] \quad (1)$$

where KSV is the Stern-Volmer constant and represents a measurement of the acrylamide ability to quench StI Trp emission and hence of its exposure to the aqueous milieu (Lakowicz, 2006). In all experiments, excitation and emission slits with 5 nm nominal band pass were used.

2.6. Binding of StI to lipid monolayers

Surface pressure (π) measurements were performed with a μTrough-S system (Kibron, Helsinki, Finland) at 23 ± 2 °C under stirring at constant area. The subphase consisted of 300 μL of 10 mM Tris–HCl, pH 7.4. Lipid monolayers were generated by applying lipid chloroformic solutions on the buffer surface to reach different initial surface pressures (π_o) in order to achieve increasing lipid:protein molar ratios. StI was then injected into the subphase following the previously described protocol (Pedrera et al., 2014).

3. Results

3.1. The presence of POPC-OOH increases StI permeabilizing activity in SM-containing vesicles

To assess the effect of including the hydroperoxized phospholipid (POPC–OOH) in lipid bilayers, we investigated GUVs composed of the well characterized lipid composition POPC:SM (1:1) (Fig. 2A upper panel), an optimal binary lipid ensemble for StI activity (Pedrera et al.,

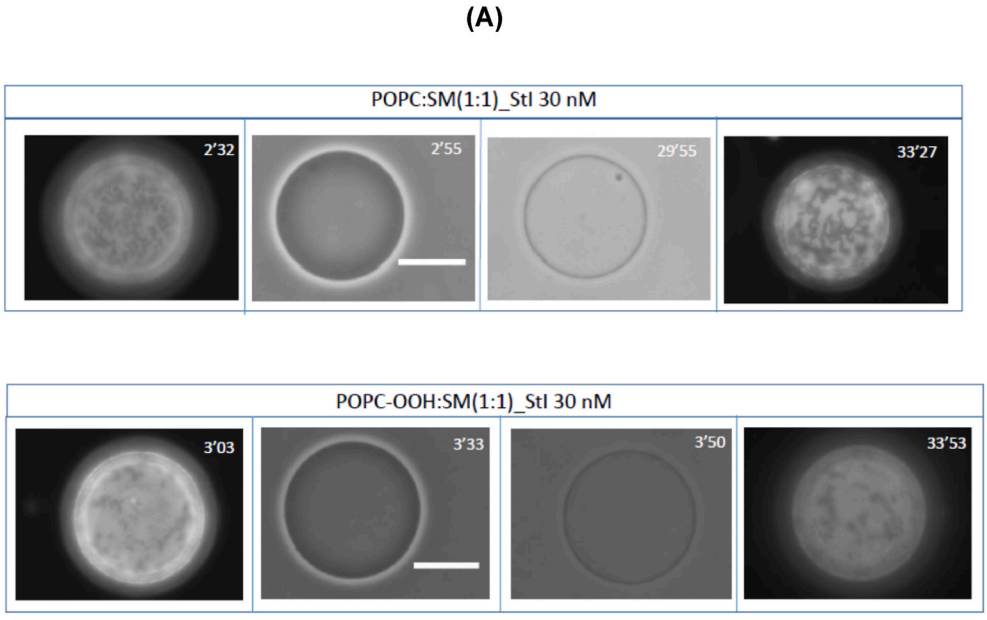

Fig. 2. Representative fluorescence (the first and last images in each row) and phase contrast images recorded from GUVs of POPC:SM (1:1) (upper row) and POPC-OOH:SM (1:1) (lower row) treated with StI (30 nM) (A). Fluorescence (the two first and last images in each row) and phase contrast images recorded from GUVs of POPC:SM (1:1) (upper row) and POPC-OOH:SM (1:1) (lower row) without StI (B). The time sequence, expressed in minutes in the right upper corner of each image, stands for the elapsed time after mixing the StI-containing glucose solution with GUVs-containing sucrose solution (A) or the addition of the glucose solution devoid of StI to GUVs-containing sucrose solution (B). StI: lipid molar ratio: ~1:200. Similarly, a consistent dependence of the results on time and lipid composition was obtained with the other StI concentrations studied (4–15 nM StI, not shown). Fluorescence images are slightly out of focus to highlight the coexistence of gel-fluid phases. The scale bars spans 20 μm.

2014; Tejuca et al., 1996), and compared with POPC-OOH:SM (1:1) (Fig. 2A, lower panel). The lipid mixture also contained 0.2 mol% of the lipophilic fluorescent dye Rho-PE that predominantly partitions into the fluid phase in the case of membranes in which different phases co-exist (Zhao et al., 2007). As can be seen, the addition of StI (30 nM) to the external GUV suspension caused a gradual decrease in the optical phase contrast of the giant POPC:SM liposomes over time, reaching a total fading in an elapsed time of circa 30 min (Fig. 2A, upper panel). Such an effect is due to the inner and outer sugar solutions exchange, reflecting an increase in lipid bilayer permeability. Given that StI is a well-known pore forming toxin, that no micron-sized pores were observed during the experiments, and considering that the microscope resolution is of few microns, this finding suggests the formation of submicrometric-sized pores by the toxin (Pedrera et al., 2015; Tejuca et al., 2001). Moreover, the permeabilizing activity of StI did not lead to the dissolution/disappearance/burst of the GUVs indicating that the permeabilization does not involve a detergent-like mechanism (Sudbrack et al., 2011). Strikingly, phase contrast fading took place in less than 4 min for GUVs made up of POPC-OOH:SM (1:1) under the influence of 30 nM StI (Fig. 2A, lower panel). Of note, control GUVs of both lipid compositions did not experience permeabilization in the absence of StI (Fig. 1B) in the experimental time course. No permeabilizing activity of StI was observed on GUVs composed solely of either POPC or POPC-OOH (Fig. S).

Interestingly, in fluorescence mode, the binary equimolar lipid mixtures show a clear gray due to the fluid phase attributed to either POPC or POPC-OOH phospholipids coexisting with dark regions of a more packed SM-based gel phase. In accordance, it was recently demonstrated that POPC-OOH can be a promoter of the liquid disordered (Ld)-liquid order (Lo) phase coexistence in membranes composed by DPPC and Chol, due to its modified oxidized molecular structure (Tsubone et al., 2019) indicating that that POPC-OOH favors lipid demixing. As one can observe from Fig. 2, although StI promotes membrane pore formation, its presence does not perturb the coexisting lipid domains boundaries over the incubation time.

3.2. The StI permeabilizing activity in POPC-OOH and SM-containing vesicles depends on the content of OxPL

In order to further verify the influence of POPC-OOH on toxin

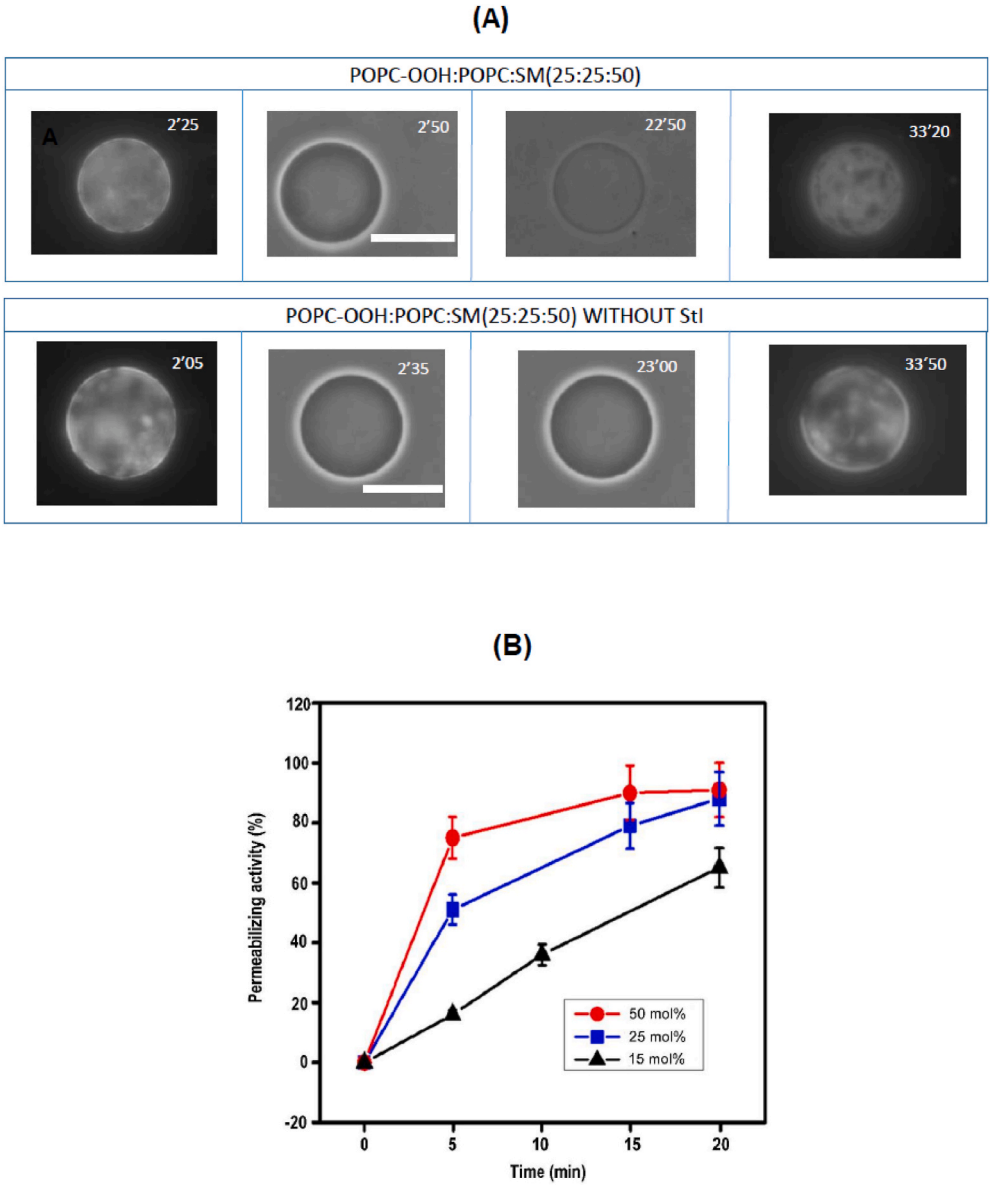

Fig. 3. Time course of the permeabilizing activity elicited by StI in GUVs.

permeabilizing activity, we assessed the effect of different StI concentrations (4–30 nM) on lipid compositions containing 50 mol% SM and variable concentrations of POPC mixed with POPC-OOH to achieve 50 mol% (POPC–OOH: 15, 25, 50 mol%). The rationale behind this design was to assess the POPC-OOH contribution to the above-described results varying its proportion in the mixture but keeping constant the SM content. This is of the outmost importance since an increase in SM up to 50 mol% promotes a proportional increase in binding and pore-formation by Sts (Pedrera et al., 2014; Tejuca et al., 1996). On the other extreme, greater SM concentrations (>50 mol%) significantly modify the physicochemical properties of the system in terms of vesicle size (Valcarcel et al., 2001) or lipid packing that would turn more difficult to interpret the results of protein action as a function of lipid composition (Pedrera et al., 2014).

Representative fluorescence images of fluid-gel phase coexistence and contrast phase loss for POPC-OOH:POPC:SM (25:25:50) exerted by StI (15 nM) are displayed in Fig. 3A. These results illustrate that increasing the proportion of the oxidized lipid in the mixture enhances the activity of the protein (Fig. 3B).

Representative images of POPC-OOH:POPC:SM (25:25:50) containing 0.2 mol% of Rho-PE and treated with 15 nM StI (upper panel) or not (lower panel) observed in fluorescence mode (first and last images in the row) and phase contrast mode. The time sequence, expressed in minutes in the right upper corner of each image, refers to the elapsed time after mixing the StI-containing glucose solution to GUVs-containing sucrose solution. The scale bars spans 20 μm (A). Permeabilization of POPC-OOH:POPC:SM (15:35:50), (triangles); POPC-OOH:POPC:SM (25:25:50), (squares); and POPC-OOH:POPC:SM (50:0:50), (circles). 0% of permeabilization stands for the initial condition upon mixture of StI with the GUVs, where the vast majority of vesicles was intact, and considered as the total amount of non-permeabilized GUVs in that microscope field. 100% refers to a condition in which all vesicles in that particular microscope field have lost optical phase contrast (B). StI:lipid molar ratio, ~1:400. Similarly, a consistent dependence of the permeabilization results on time and lipid composition was obtained with the other StI concentrations studied (4, 7 and 30 nM StI, not shown). GUVs of the four compositions studied but without StI (controls) were followed over 30 min and no phase contrast or modification of phase landscape was observed. Values are expressed as the mean and standard deviation determined from three independent experiments.

Importantly, in our study, inclusion of 15, 25 or 35 mol% POPC-OOH in POPC:SM vesicles keeping constant SM concentration (50 mol%), POPC-OOH:POPC:SM (25:25:50) (Fig. 3A lower panel), or POPC-OOH in POPC-OOH: SM (50:50) (Fig. 2B, lower panel) did not result in spontaneous permeabilization of the vesicles in the absence of StI. The increase in the permeabilizing activity of StI on GUVs containing POPC-OOH and SM might be caused by *i.* the particular characteristics of the phase separation borders between the POPC-OOH enriched fluid – SM enriched gel phases and/or *ii.* the physical properties of the more fluid POPC-OOH enriched phase (Sankhagowit et al., 2014).

In order to verify whether differences in GUVs permeation could result from differences in StI binding promoted by distinct interfaces or post-binding steps we used LUVs and lipid monolayers as model membrane systems of selected lipid compositions. These are relatively simple and informative models that have been thoroughly used in our laboratory to characterize binding of Sts to membranes (Antonini et al., 2014; Martinez et al., 2001; Martínez et al., 2007; Pedrera et al., 2014, 2015).

3.3. OxPL POPC-OOH does not appear to increase StI binding to SM-containing LUVs

3.3.1. LUVs characterization

LUVs as membrane models have the advantage that can be characterized by spectroscopic approaches, as compared to the larger GUVs used in microscopy studies. The difference in curvature between both vesicle models can be considered irrelevant because LUVs have no significant curvature stress and thus there is a similar lipid distribution between the two leaflets. Moreover, any other difference derived from lipid packing is not expected; therefore, results are comparable to those obtained with GUVs (Goñi et al., 2008).

We here characterized LUVs made up of POPC:SM (1:1) and POPC-OOH:SM (1:1) in terms of size and ζ potential by DLS.

Both vesicles obtained by the extrusion procedure with polycarbonate filters with nominal holes of 100 nm rendered rather homogeneous populations in terms of size indicated by low polydispersity index (PI: 0.05–0.16). LUVs exhibited a Gaussian diameter distribution displaying a mean value of around 125 nm and low standard deviation of ~5 nm. Further, all vesicles exhibited ζ potential values around −30 mV. Therefore, POPC-hydroperoxidation did not impact on membrane surface charge nor on LUVs size.

3.3.2. The enhancement of StI activity cannot be ascribed to a higher binding extent to POPC-OOH-SM-containing LUVs as perceived by fluorescence spectroscopy

It is well recognized that the mechanism of pore-formation by actinoporins involves several stages, i.e. membrane binding, oligomerization, N-terminus detachment of the protein body and its insertion into the hydrophobic core of the bilayer, and eventually pore formation (Rojko et al., 2013, 2016). The first step in this sequence of events is the association of the soluble monomers to the membrane (Alvarez et al., 2017; Castrillo et al., 2010; Mancheño et al., 2003). The relatively high concentration of Trp and Tyr in the Sts' binding region (Castrillo et al., 2010; Mancheño et al., 2003) enables the use of fluorescence spectroscopy in the assessment of protein binding to membrane (Alvarez et al., 2003; Martínez et al., 2007). Association to membrane involves an increase in the fluorescence intensity and a shift of its emission maximum to shorter wavelengths; both phenomena result from the modification of the microenvironment of aromatic amino acids shifted from a polar to a more apolar milieu in membrane (Lakowicz, 2006). In order to investigate whether the increase in the permeabilization activity of StI observed in GUVs of lipid compositions containing SM and the OxPL POPC-OOH could be ascribed to the binding step, we performed binding studies on LUVs of the same basic lipid compositions examined by fluorescence microscopy (Fig. 2). Binding of the toxin to liposomes was followed by collecting the intrinsic fluorescence of the StI's Trp residues upon excitation at $\lambda = 295$ nm in solution and in the presence of increasing liposome concentrations. The spectra of StI in the presence of vesicles comprising POPC:SM (50:50) and POPC-OOH:SM (50:50) show emission maxima blue-shifted (approximately 15 nm) accompanied by an increased fluorescence intensity when compared to StI in solution (Fig. 4A). This behavior reflects an average less exposure of Trp residues towards the aqueous external medium upon vesicle addition. In contrast, in the presence of vesicles lacking SM (either POPC or POPC-OOH), StI spectra does not experience increase in the emission intensity or a shift towards lower wavelengths (results not shown). This would be indicating that StI does not bind significantly to these two systems lacking SM as previously reported (Tejuca et al., 1996). It is interesting to point out that in the presence of vesicles containing POPC-OOH and lacking SM, the intensity of the fluorescence is even lower than that of StI (not shown) probably due to a quenching effect promoted by this OxPL. This could be also the case for the composition POPC-OOH:SM when compared to POPC:SM (Fig. 4A). The F/Fo ratio for increasing selected StI:lipid molar ratios show an increase for both lipid compositions but is visibly higher for vesicles that do not contain the peroxidized phospholipid (Panel B in Fig. 4). The smaller and no consistent increase in the ratio for POPC-OOH-containing vesicles may result from the quenching of StI Trp fluorescence as mentioned above. This is supported by the fact that Trp residues tend to accommodate mainly in lipid-water interface (De Planque et al., 2003) as it has also been proposed for actinoporins (García-Linares et al., 2016). It is noteworthy that in both types of vesicles, the maximum fluorescent emission is around the same values and shifted towards lower wavelengths when compared to StI in

A

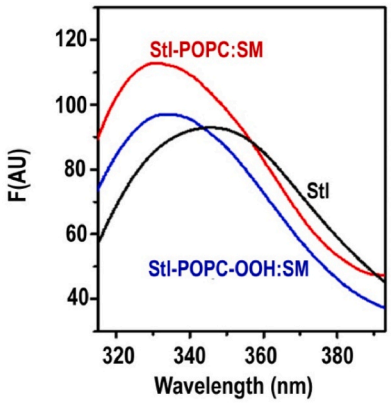

B

L:StI (molar ratio)	F/F$_o$ POPC:SM (1:1)	F/F$_o$ POPC-OOH:SM (1:1)
50	1.10	1.15
70	1.25	1.06
200	1.40	1.22

Composition	Ksv (M^{-1})
StI	6.49 ± 0.53
StI + POPC:SM	1.16 ± 0.13
StI + POPC-OOH:SM	1.00 ± 0.12

C

Fig. 4. Binding of StI to liposomes of POPC:SM (50:50) and POPC-OOH:SM (50:50). Typical intrinsic fluorescence spectra of StI in solution (1.5 μM) and in the presence of LUVs. LUVs were added in increasing concentrations and StI fluorescence spectra recorded For clarity, only spectra collected at an appropriate lipid: protein molar ratio (~100:1) is presented (A). LUVs of other lipid compositions e.g. POPC, POPCOOH were examined but no relevant StI binding was recorded. F/Fo values for increasing lipid (L):StI molar ratios (B). SternVolmer constants (Ksv) calculated from the quenching by acrylamide assays of StI in solution and bound to liposomes of the indicated compositions at saturating vesicle concentration (values are expressed as the mean ± standard deviation; quenching linear fit according to Eq (1) ($r^2 > 0.98$) (C). All measurements were carried out in triplicate in a spectrofluorimeter Varian, Cary-Eclipse at T = 22 ± 2 °C in buffer 10 mM Tris-HCl, pH 7.4. Spectra were corrected for light dispersion by LUVs. Spectra were collected after excitation of StI Trp residues at 295 nm. Slit widths of 5 nm were used for excitation and emission beams. A.U., Arbitrary Units, F/Fo: is the ratio between StI fluorescence in the presence (F) and absence (Fo) of LUVs.

solution, indicative of StI binding to the membrane (Panel A in Fig. 4).

Selective Trp fluorescence quenching by the hydrophilic quencher acrylamide is used to estimate the exposure of the emitting centers to the aqueous milieu or to the lipid environment. Quenching studies in conjunction with binding isotherms provide useful information on actinoporin binding to membranes (Alvarez et al., 2003; Macek et al., 1995; Martinez et al., 2001). The fluorescence quenching study with acrylamide revealed, as expected, that on average StI's Trp residues are more exposed to the external medium when the protein is in solution than in the presence of both types of vesicles (POPC–OOH:SM and POPC:SM). In accordance, the Ksv values calculated by expression (1) were lower for StI in the presence of both types of vesicles because of a less access to water of Trp residues, which indicates binding of StI to LUVs. Interestingly both Ksv values were similar for the SM-containing vesicles (Panel C in Fig. 4).

Is summary, this fluorescence studies show that the replacement of POPC in liposome composition by POPC-OOH does not alter the StI binding to SM-containing membranes. However, the presence of the –OOH moiety oriented towards the water-membrane interface where StI Trp residues are located (Mancheño et al., 2003) might be quenching the fluorescence of Trp residues adding some uncertainty to these results. In fact, protonated carboxyl groups near Trp residues have been identified among the factors that quench the emission from Trp residues due to their electron acceptor ability (Lakowicz, 2006). For this reason, we decided to study binding of StI to Langmuir lipid monolayer systems of the same compositions. These studies allow for obtaining additional information on the binding of StI to the membrane based on other physical principle circumventing the uncontrolled phenomena associated with fluorescence quenching.

3.4. StI binding to lipid monolayers

To assess binding of StI to lipid monolayer, we followed the time course of the surface pressure increase after adding StI to the aqueous subphase (Fig. 5A). Plotting the increase in the surface pressure as a function of time revealed different profiles for the equimolar PC:SM and POPC-OOH:SM mixtures for the same initial pressure (~18 mN m^{-1}) upon the addition of the same protein concentration. While the curve corresponding to the mixture POPC:SM displays a stepwise increase in the signal after the initial upsurge (first 25 s), the response of the surface pressure of the POPC-OOH:SM monolayer exhibits the same initial jump (first 25 s) followed by an approximate constant value (~26 mN m^{-1}) until ~130 s. After that, the signal increases progressively up to saturation reaching similar values than its POPC:SM counterpart at equilibrium (Fig. 5A). Interestingly, in a recent work, it was demonstrated by time resolved fluorescence experiments that the presence of POPC-OOH in lipid bilayers results in a higher microviscosity in the close proximity to the –OOH moiety, i. e, in the polar/apolar interface (Scanavachi et al., 2021). Taking into account such result, and the fact that Trp residues essential for binding are probably located in the vicinity of the.

POPC-OOH, we might infer that the increase in the local viscosity near the hydroperoxide group could interfere in the StI insertion in the POPC-OOH:SM monolayer in the initial binding stage and afterwards, reflected by a gradual surface pressure increase over interaction time in comparison to the surface pressure profile exhibited by StI association to POPC:SM monolayer.

From the time profiles of the increase in π following StI addition at varying initial pressures of the lipid monolayer, as those shown in Fig. 5A, we calculated the critical pressure (π_c) obtained by extrapolating to zero the upsurge in surface pressure ($\Delta\pi$) as a function of the initial pressure (π_o). This parameter characterizes the pressure that must be applied to avoid binding of the toxin to the monolayer and is directly correlated with the binding of the protein to the lipid system (Brockman, 1999). Those compositions containing SM (Fig. 5B) show the highest critical pressure values when compared to those monolayers lacking the sphingolipid (POPC: $\pi_c = 43 \pm 4$ mN m^{-1} and POPC-OOH: $\pi_c = 40.4 \pm 3$ mN m^{-1}). The increase in surface pressure resulting from the association of the toxin to previously formed lipid systems showed in all cases π_c values larger than 35 mN m^{-1}. This value has been associated to the lateral pressure of a typical biological membrane (Brockman, 1999). It has been suggested that, when the π_c is higher than this critical value, the protein not only binds to the lipid monolayer, but also penetrates it (Caaveiro et al., 2001). For all the examined compositions, π_c values were higher than 35 mN m^{-1} suggesting that the toxin is able to

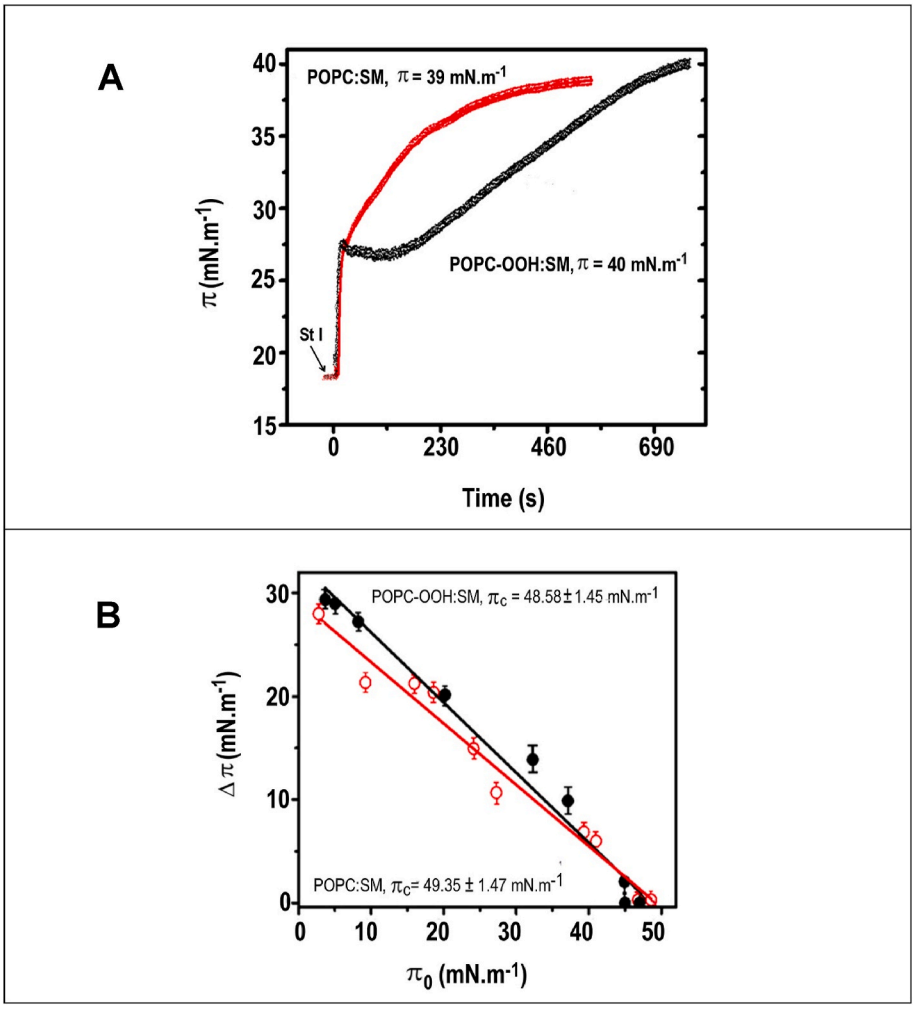

Fig. 5. Binding of StI to lipid monolayers. The increase in surface pressure was registered with constant stirring at constant area, as a function of time, until a stable signal was obtained. Representative timecourse profiles for POPC:SM (1:1) upper red line and POPC-OOH:SM (1:1) lower black line (A). Critical pressures (π_c) were calculated by extrapolating regression lines from $\Delta\pi$ vs. π_o plots as shown in (B). StI concentration in the subphase: 0.9 μM. Values were obtained after equilibration under gentle stirring and expressed as the mean value ± the standard deviation of at least 3 independent experiments. The line represents the best linear fit of data ($r^2 = 0.96$). POPC-OOH:SM (1:1) black line, POPC:SM (50:50) red line. T = 23 ± 2 °C in buffer 10 mM Tris-HCl, pH 7.4. (For interpretation of the references to colour in this figure legend, the reader is referred to the Web version of this article.)

penetrate all these lipid systems. Strikingly, the presence of SM favors to the same extent StI binding irrespectively of the PC used, POPC/POPC-OOH, or possible differences in lateral organization of the monolayer derived from the mixing of both PC species and SM, although the mechanisms of StI insertion in the monolayers differ as shown in Fig. 5A.

4. Discussion

Over the last decade, multiple advances have been made in understanding the structure–function relationship and the influence of membrane properties on actinoporin functionality; however, to the best of our knowledge, this is the first report on the impact of an oxidized lipid on the pore-forming activity of a member of this PFTs family. Therefore, in this work our interest was to explore the impact of the presence of an oxidized lipid on the activity of StI trying to clarify how the membrane properties modified by this OxPL (membrane interface, phase coexistence, lipid packing) modulate StI action.

The experimental approach followed in this work, supported by its use in a variety of studies (Jurkiewicz et al., 2012; Rosa et al., 2018; Siani et al., 2016), consisted in incorporating an oxidized PC bearing a hydroperoxide group into lipid model systems. With this in mind, we assessed StI binding and permeabilizing activity on diverse model membrane systems containing POPC-OOH.

Firstly, we examined the permeabilizing activity of StI on GUVs following the loss of optical phase contrast. The incorporation of the hydroperoxidized lipid in SM-containing membranes enhanced the activity of the toxin as compared to the mixture including the non-oxidized POPC and SM (Fig. 2A). This membrane destabilization was not due to spontaneous vesicle leaking since no contrast phase loss was observed in the absence of the toxin, at least in the time scale of our experiments (Fig. 2B). Moreover, this result is consistent with previous observations describing that the occurrence of hydroperoxide groups in the lipid bilayer does not increase membrane permeability or promote pore formation (Rosa et al., 2018; Siani et al., 2016; Weber et al., 2014). It should be noted that the permeabilization of GUVs by StI kept the vesicles intact even after a long time of exposure to the protein (>1hr) or with the use of high protein concentration (50 nM). In no case the dissolution or bursting of the vesicles, typical of a detergent-like mechanism of action (Sudbrack et al., 2011), was observed under these conditions, which excludes that the action of StI is due to a detergent-type mode of action. Therefore, the increase in membrane permeability can be ascribed to the pore forming activity of StI as we have previously demonstrated in GUVs or LUVs of other compositions (Martínez et al., 2007; Pedrera et al., 2015; Tejuca et al., 1996, 2001; Valcarcel et al., 2001). It is worth to point out that both POPC:SM and POPC-OOH:SM (1:1) GUVs exhibited lateral phase separation (Fig. 2). This landscape comprises the coexistence of a fluid phase enriched in POPC/POPC-OOH and other more packed phase, predominantly composed of SM. The presence of irregular borders in the darker phase is a typical characteristic of solid ordered phases (So) (Veatch and Keller, 2003); therefore, in the binary systems apparently coexist a fluid phase and a more organized solid ordered (So) one (Fig. 2). This is supported by the fact that in GUVs, solid domains coexisting with liquid phase

strongly exclude the fluorescent probe, are commonly noncircular and rotate as rigid entities in a background of a liquid phase (Veatch and Keller, 2003).

The hydroperoxide group present in POPC-OOH due to its hydrophilic character tends to migrate to the bilayer surface eliciting an increase in the lipid molecular area and a decrease in the bilayer thickness and order parameters (Jurkiewicz et al., 2012; Wong-Ekkabut et al., 2007); this increase in molecular area leads to an increase in the lateral area of the membrane (Beranova et al., 2010; Khandelia and Mouritsen, 2009; Sankhagowit et al., 2014; Wong-Ekkabut et al., 2007). In fact, small angle X-ray scattering and molecular dynamics studies with different oxidized lipid species included in model lipid bilayer systems revealed that hydroperoxidized groups tend to be usually located near the headgroup region (Garrec et al., 2014; Siani et al., 2016; Wong-Ekkabut et al., 2007) due to transient hydrogen bonding with water, carbonyl, and phosphate groups conferring a larger area per lipid. The increase of the average area per lipid due to the presence of –OOH groups can hinder the packing between the different lipids and prompt phase separation (Tsubone et al., 2019).

Meanwhile, experimental studies with GUVs revealed that the hydroperoxide groups significantly impact on membrane properties as, for instance, increase in lateral area (Haluska et al., 2012; Riske et al., 2009) in good agreement with molecular dynamics data (Tsubone et al., 2019), fluidity (Sankhagowit et al., 2014), elastic modulus (Weber et al., 2014) and rafts reorganization (Tsubone et al., 2019).

Of note, the modifications to the physical properties of the bilayer introduced by POPC-OOH are not sufficient to promote StI permeabilizing activity; in fact, vesicles composed exclusively of this peroxidized lipid were not sensitive to the permeabilizing activity of the toxin (Fig. S). This is not surprising, given the specific role assigned to SM in membrane binding and pore-formation by StI (Tejuca et al., 1996; Valcarcel et al., 2001); even more, it has been recently demonstrated that SM besides its role as lipid receptor of actinoporins, it also can act as a structural element of the pore, where it functions as an assembly co-factor (Tanaka et al., 2015).

The increased activity of Sts does not seem to depend on a significant enhanced binding to membrane at least as evidenced from LUVs results by fluorescence spectroscopic assays (Fig. 4). Regarding the monolayer experiments, the toxin association to the monolayer of POPC-OOH:SM revealed a different mechanism of insertion to that of POPC:SM. After a similar initial binding rate, the accommodation of the toxin into the POPC-OOH:SM monolayer takes a longer time, but once this stage has been overcome, the protein finally integrates into the monolayer reaching a similar surface tension value following long interaction time (Fig. 5). The pore-forming mechanism of actinoporins can be dissected into two major steps: a first one regarding binding to membrane and a second one related to the organization of monomers into a functional multimeric pore (Rojko et al., 2016). Assuming this simplified framework, studies with lipid monolayers besides being considered classical indicators of the actinoporins binding extent to the lipid ensemble, they also may reflect somehow the influence of the final steps leading to pore–formation. Therefore, different kinetic profiles (Fig. 5A) must be reflecting diverse ways to approximate to the final state in the membrane probably due to the influence of the hydroperoxidized group in the membrane.

Membrane packing properties could be an important factor in the oligomerization step and the penetration of the N-terminal region of the toxin into the lipid membrane, since both processes involve the lateral displacement and rearrangement of lipid components. In this sense, we have previously observed that when binding is not a limiting factor (i.e. at saturating lipid conditions, manuscript submitted), membrane fluidity also potentiated vesicle permeabilization. In other words, membrane fluidity plays an important role for the effectiveness of the post-binding processes including oligomerization and membrane insertion that result in the formation of the lytic structure in the membrane. Others have observed that under optimal binding conditions, the rate–limiting step would involve the subsequent steps mandatory to produce the pore, once the actinoporin is associated to the membrane (Garcia-Linares et al., 2016). According to our fluorescence spectroscopy results, StI binding extent to POPC-OOH:SM and POPC:SM membranes is equivalent (Fig. 4), although through different pathways as revealed by surface tension data (Fig. 5). Therefore, we infer that the higher permeabilizing activity of StI in POPC-OOH:SM membranes does not derive from a higher affinity to this lipid ensemble. Moreover, all the examined compositions contain a fixed and high proportion of SM (50 mol%); therefore, they are excellent targets for StI binding, irrespective of the phosphatidylcholine type (POPC or POPC-OOH). This would explain why minor differences in binding leading to pore-formation are difficult to be recorded. However, the looser lipid packing imposed by this OxPL in the fluid phase (and in the borders of phase coexistence) coupled to the presence of –OOH groups at polar/apolar interface seem to facilitate the toxin diffusion and/or oligomerization towards pore formation.

Of note, the presence of phase separation in oxidized PC:SM membranes does not enhance significantly StI binding when compared to POPC:SM membranes at least in the steady-state conditions reached in the fluorescence and lipid monolayer studies. This is consistent with our previous results with ternary systems of PC:SM:sterol with phase coexistence (cholesterol/ergosterol) or not (cholestenone). From these studies we concluded that sterols favor StI-membrane association irrespective of their ability to generate laterally segregated domains (Pedrera et al., 2015). It has been shown that binding of EqtII to the lateral interfaces between Ld-Lo coexisting phases is a transient phenomenon; in this way, the toxin initially binds to the lateral interfaces and from there diffuses into the Ld phase (Rojko et al., 2014). Here, if one assumes that the toxin distribution occurs according to its concentration gradient from the phase boundaries, then the larger and less ordered phase would appear with a higher proportion of toxin facilitating pore-formation leading to vesicle permeabilization. In summary, most probably, the phase boundaries of both POPC:SM (1:1) and POPC-OOH:SM (1:1) mixtures as well as the coexisting phases are sufficiently attractive for StI binding given their high SM content, hence the properties of the less packed phase coupled to the presence of –OOH group in the membrane interface, in this case the POPC-OOH enriched phase, should play a prominent role in the permeabilizing activity of StI.

More recently, it was demonstrated at atomic level that the pore originated by the actinoporin FraC shows a peculiar architecture composed of lipids and proteins, where some of the lipids lining the pore wall act as assembly cofactors. The predominant transmembrane pore of FraC in DOPC/SM vesicles was an 8-mer with the aqueous channel exhibiting 8 lateral fenestrations (windows) in the walls of the pore one at each protomer–protomer contact interface (Tanaka et al., 2015). Due to the plasticity of the lipid binding sites of FraC it is tempting to speculate that other lipids bearing the same headgroup, that is, phosphorylcholine, such as POPC-OOH could occupy any of these sites and positively modify the organization of the pore in actinoporins. Since lipids play an important role in pore organization, it will be interesting to assess if the composition of the acyl-chain of a phosphorylcholine-bearing lipid such as POPC-OOH or SM or even the nature of the headgroup of the lipid rules the pore stoichiometry and hence the activity of the protein.

5. Conclusions

Here we have demonstrated that the combination of the OxPL POPC-OOH with SM renders vesicles more susceptible to the pore-forming activity of StI when compared to those of POPC:SM. This boosted activity does not seem to be the consequence of a preferential binding to the lipid ensemble containing the OxPL; rather it is probably due to the changes in the less ordered phase of the hydrophobic medium promoted by POPC-OOH when compared to the non-oxidized PC counterpart. Once in the membrane, the subsequent events leading to pore-formation

might be facilitated by the higher fluidity of the POPC-OOH-enriched domain. Work is in progress in our laboratory in order to visualize the location of StI in these vesicles and the contribution of other OxLs to the activity of this PFP.

Credit author statement

Carlos Alvarez: Conceptualization, Formal analysis, Resources, Investigation, Data curation, Writing – original draft preparation, review and editing, Visualization, Funding acquisition, Supervision and project administration. Rosangela Itri: Conceptualization, Formal analysis, Resources, Investigation, Data curation, writing-review and editing, Visualization, Funding acquisition, Supervision and project administration. María E. Lanio: Formal analysis, Data curation, writing-review and editing, Visualization, and supervision. Carmen Soto: Investigation, Formal analysis, Data curation, writing-review and editing, and visualization. Maressa Donato: Investigation, Formal analysis, Data curation, writing-review and editing, and visualization.

Declaration of competing interest

The authors declare that they have no known competing financial interests or personal relationships that could have appeared to influence the work reported in this paper.

Acknowledgements

Authors thank to São Paulo Research Foundation (FAPESP) (2016/01379–1, 2017/08460–1), Brazi, and to Cuban National Program on Basic and Natural Sciences (PNCBN– PN223LH010-008) for financial support. MD was recipient from National Council for Scientific and Technological Development (CNPq) undergraduate fellowship. RI is recipient from CNPq research fellowship. Thanks to Julio Pérez Erviti for assistance in StI representation.

Caption to supplementary figure

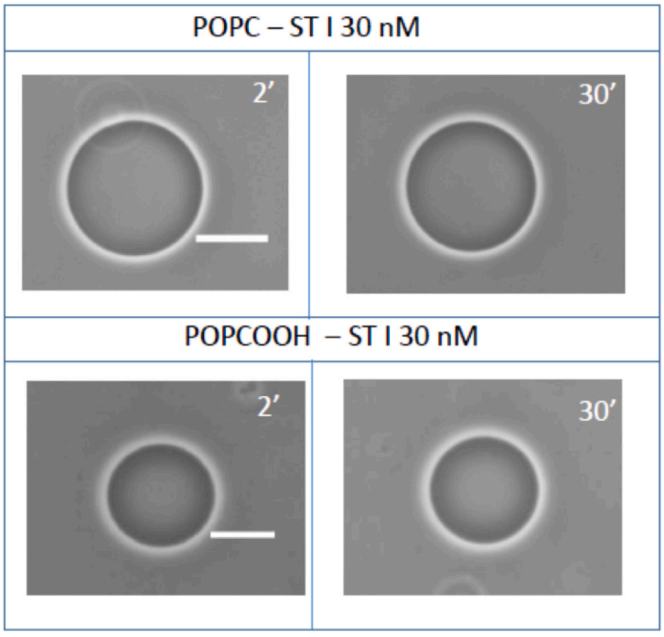

Fig. S. Phase contrast images recorded from GUVs of POPC (upper row) and POPC-OOH (lower row) treated with 30 nM StI at 2 and 30 min. This refers to the elapsed time after mixing the StI-containing glucose solution to GUVs-containing sucrose solution. The scale bars spans 20 μm.

References

Alegre-Cebollada, J., Rodríguez-Crespo, I., Gavilanes, J.G., del Pozo, A.M., 2006. Detergent-resistant membranes are platforms for actinoporin pore-forming activity on intact cells. FEBS J. 273, 863–871. https://doi.org/10.1111/j.1742-4658.2006.05122.x.

Alvarez, C., Casallanovo, F., Shida, C.S., Nogueira, L.V., Martinez, D., Tejuca, M., Pazos, I.F., Lanio, M.E., Menestrina, G., Lissi, E., Schreier, S., 2003. Binding of sea anemone pore-forming toxins sticholysins I and II to interfaces - modulation of conformation and activity, and lipid-protein interaction. Chem. Phys. Lipids 122, 97–105. https://doi.org/10.1016/S0009-3084(02)00181-0.

Álvarez, C., Mancheño, J.M., Martínez, D., Tejuca, M., Pazos, F., Lanio, M.E., 2009. Sticholysins, two pore-forming toxins produced by the Caribbean Sea anemone Stichodactyla helianthus: their interaction with membranes. Toxicon 54, 1135–1147. https://doi.org/10.1016/j.toxicon.2009.02.022.

Alvarez, C., Pazos, F., Soto, C., Laborde, R., Lanio, M.E., 2020. Pore-forming toxins from sea anemones: from protein membrane interaction to its implications for developing biomedical applications. In: Iglic, A., Rappolt, M., Garcia-Saez, A.J. (Eds.), Advances in Biomembranes and Lipid Self-Assembly, ume 31. Elsevier Inc., London, San Diego, Cambridge, Oxford, pp. 129–183. https://doi.org/10.1016/bs.abl.2020.02.005.

Alvarez, C., Ros, U., Valle, A., Pedrera, L., Soto, C., Hervis, Y.P., Cabezas, S., Valiente, P. A., Pazos, F., Lanio, M.E., 2017. Biophysical and biochemical strategies to understand membrane binding and pore formation by sticholysins, pore-forming proteins from a sea anemone. Biophys. Rev. 9, 529–544. https://doi.org/10.1007/s12551-017-0316-0.

Anderluh, G., Lakey, J.H., 2008. Disparate proteins use similar architectures to damage membranes. Trends Biochem. Sci. 33, 482–490. https://doi.org/10.1016/j.tibs.2008.07.004.

Anderluh, G., Macek, P., 2002. Cytolytic peptide and protein toxins from sea anemones (Anthozoa: actiniaria). Toxicon 40, 111–124. https://doi.org/10.1016/s0041-0101(01)00191-x.

Angelova, M.I., Dimitrov, D.S., 1986. Liposome electro formation. Faraday Discuss. Chem. Soc. 81, 303–311. https://doi.org/10.1039/DC9868100303.

Antonini, V., Pérez-Barzaga, V., Bampi, S., Pentón, D., Martínez, D., Dalla Serra, M., Tejuca, M., 2014. Functional characterization of sticholysin I and W111C mutant reveals the sequence of the actinoporin's pore assembly. PLoS One 9, e110824. https://doi.org/10.1371/journal.pone.0110824.

Bakrac, B., Anderluh, G., 2010. Molecular mechanism of sphingomyelin-specific membrane binding and pore formation by actinoporins. Adv. Exp. Med. Biol. 677, 106–115.

Barlic, A., Gutiérrez-Aguirre, I., Caaveiro, J.M., Cruz, A., Ruiz-Arguello, M.B., Perez-Gil, J., Gonzalez-Mañas, J.M., 2004. Lipid phase coexistence favors membrane

insertion of equinatoxin-II, a pore-forming toxin from Actinia equina. J. Biol. Chem. 279, 34209–34216. https://doi.org/10.1074/jbc.M313817200.
Beranova, L., Cwiklik, L., Jurkiewicz, P., Hof, M., Jungwirth, P., 2010. Oxidation changes physical properties of phospholipid bilayers: fluorescence spectroscopy and molecular simulations. Langmuir 26, 6140–6144. https://doi.org/10.1021/la100657a.
Bernheimer, A.W., Avigad, L.S., 1976. Properties of a toxin from the sea anemone Stoichactis helianthus, including specific binding to sphingomyelin. Proc. Natl. Acad. Sci. U. S. A 73, 467–471. https://doi.org/10.1073/pnas.73.2.467.
Brockman, H., 1999. Lipid monolayers: why use half a membrane to characterize protein- membrane interactions? Curr. Opin. Struct. Biol. 9, 438–443. https://doi.org/10.1016/S0959-440X(99)80061-X.
Caaveiro, J.M., Echabe, I., Gutierrez, I., Nieva, L., Arrondo, L., Gonzalez-Manas, J.M., 2001. Differential interaction of equinatoxin II with model membranes in response to lipid composition. Biophys. J. 80, 1343–1353. https://doi.org/10.1016/S0006-3495(01)76107-3.
Castrillo, I., Araujo, N.A., Alegre-Cebollada, J., Gavilanes, J.G., Martínez-del-Pozo, A., Bruix, M., 2010. Specific interactions of sticholysin I with model membranes: an NMR study. Proteins Struct. Funct. Bioinforma. 78, 1959–1970. https://doi.org/10.1002/prot.22712.
Corvalán, N.A., Caviglia, A.F., Felsztyna, I., Itri, R., Lascano, R., 2020. Lipid hydroperoxidation effect on the dynamical evolution of the conductance process in bilayer lipid membranes: a condition toward criticality. Langmuir 36, 8883–8893. https://doi.org/10.1021/acs.langmuir.0c01243.
De Planque, M.R.R., Bonev, B.B., Demmers, J.A.A., Greathouse, D.V., Koeppe, R.E., Separovic, F., Watts, A., Killian, J.A., 2003. Interfacial anchor properties of tryptophan residues in transmembrane peptides can dominate over hydrophobic matching effects in peptide-lipid interactions. Biochemistry 42, 5341–5348. https://doi.org/10.1021/bi027000r.
Devlin, J.P., 1974. Isolation and partial purification of hemolytic toxin from sea anemone, Stoichactis helianthus. J. Pharmacol. Sci. 63, 1478–1480. https://doi.org/10.1002/jps.2600630936.
Dos Santos, A.G., César, J.C., Dufour, G., Cataldo, D., Evrard, B., Silva, L.C., Deleu, M., Mingeot-Leclercq, M.-P., 2017. Changes in membrane biophysical properties induced by the Budesonide/Hydroxypropyl- β -cyclodextrin complex. Biochim. Biophys. Acta Biomembr. 1859 https://doi.org/10.1016/j.bbamem.2017.06.010, 1930–1940.
Doyle, J., Kem, W., Villalonga, F., 1989. Interfacial activity of an ion channel-generating protein cytolysin from the sea anemone stichodactyla helianthus. Toxicon 27, 465–471.
Drechsler, A., Anderluh, G., Norton, R.S., Separovic, F., 2010. Solid-state NMR study of membrane interactions of the pore-forming cytolysin , equinatoxin II. BBA - Biomembr 244–251. https://doi.org/10.1016/j.bbamem.2009.10.012, 1798.
García-Linares, S., Castrillo, I., Bruix, M., Menéndez, M., Alegre-Cebollada, J., Martínez-del-Pozo, Á., Gavilanes, J.G., 2013. Three-dimensional structure of the actinoporin sticholysin I. Influence of long-distance effects on protein function. Arch. Biochem. Biophys. 532, 39–45. https://doi.org/10.1016/j.abb.2013.01.005.
García-Linares, S., Maula, T., Rivera-De-Torre, E., Gavilanes, J.G., Slotte, J.P., Martínez-Del-Pozo, Á., 2016. Role of the tryptophan residues in the specific interaction of the sea anemone stichodactyla helianthus's actinoporin sticholysin II with biological membranes. Biochemistry 55, 6406–6420. https://doi.org/10.1021/acs.biochem.6b00935.
Garcia-Linares, S., Rivera-de-Torre, E., Morante, K., Tsumoto, K., Caaveiro, J.M., Gavilanes, J.G., Slotte, J.P., Martinez-del-Pozo, A., 2016. Differential Effect of Membrane Composition on the Pore – Forming Ability of Four Different Sea Anemone Actinoporins, vol. 55, pp. 6630–6641. https://doi.org/10.1021/acs.biochem.6b01007.
Garrec, J., Monari, A., Assfeld, X., Mir, L.M., Tarek, M., 2014. Lipid peroxidation in membranes: the peroxyl radical does not float. J. Phys. Chem. Lett. 5, 1653–1658. https://doi.org/10.1021/jz500502q.
Goñi, F.M., Alonso, A., Bagatolli, L.A., Brown, R.E., Marsh, D., Prieto, M., Thewalt, J.L., 2008. Phase diagrams of lipid mixtures relevant to the study of membrane rafts. Biochim. Biophys. Acta 1781, 665–684. https://doi.org/10.1016/j.bbalip.2008.09.002.
Haluska, C.K., Baptista, M.S., Fernandes, A.U., Schroder, A.P., Marques, C.M., Itri, R., 2012. Photo-activated phase separation in giant vesicles made from different lipid mixtures. Biochim. Biophys. Acta Biomembr. 1818, 666–672. https://doi.org/10.1016/j.bbamem.2011.11.025.
Hong, Q., Gutiérrez, I., Barlic, A., Malovrh, P., Kristan, K., Podlesek, Z., Macek, P., Turk, D., González-Mañas, J.M., Lakey, J.H., Anderluh, G., 2002. Two-step membrane binding by equinatoxin II , a pore-forming toxin from the sea anemone , involves an exposed aromatic cluster and a flexible helix. J. Biol. Chem. 277, 41916–41924. https://doi.org/10.1074/jbc.M204625200.
Itri, R., Junqueira, H.C., Mertins, O., Baptista, M.S., 2014. Membrane changes under oxidative stress : the impact of oxidized lipids. Biophys. Rev . 6, 47–61. https://doi.org/10.1007/s12551-013-0128-9.
Jurkiewicz, P., Olzynska, A., Cwiklik, L., Conte, E., Jungwirth, P., Megli, F.M., Hof, M., 2012. Biophysics of lipid bilayers containing oxidatively modified phospholipids: insights from fluorescence and EPR experiments and from MD simulations. Biochim. Biophys. Acta 1818, 2388–2402. https://doi.org/10.1016/j.bbamem.2012.05.020.
Kem, W.R., 1988. The Biology of Nematocysts, the Biology of Nematocysts. Elsevier Inc. https://doi.org/10.1016/B978-0-12-345320-4.X5001-9.
Khandelia, H., Mouritsen, O.G., 2009. Lipid gymnastics: evidence of complete acyl chain reversal in oxidized phospholipids from molecular simulations. Biophys. J. 96, 2734–2743. https://doi.org/10.1016/j.bpj.2009.01.007.
Lakowicz, J.R., 2006. Principles of Fluorescence Spectroscopy. In: Book, third ed. ed. Springer International Publishing, Berlin. https://doi.org/10.1117/1.2904580.
Lanio, M.E., Morera, V., Alvarez, C., Tejuca, M., Gómez, T., Pazos, F., Besada, V., Martínez, D., Huerta, V., Padrón, G., Chávez, M.A., 2001. Purification and characterization of two hemolysins from Stichodactyla helianthus. Toxicon 39, 187–194. https://doi.org/10.1016/S0041-0101(00)00106-9.
Linder, R., Bernehimer, A., Kim, K.-S., 1977. Interaction between sphingomeylin and a cytolysin from the sea anemone Stoichactis helianthus. Biochim. Biophys. Acta 467, 290–300. https://doi.org/10.1016/0005-2736(77)90306-6.
Macek, P., Zecchini, M., Pederzolli, C., Dalla Serra, M., Menestrina, G., 1995. Intrinsic tryptophan fluorescence of equinatoxin II, a pore-forming polypeptide from the sea anemone Actinia equina L, monitors its interaction with lipid membranes. Eur. J. Biochem. 234, 329–335.
Malovrh, P., Viero, G., Dalla Serra, M., Podlesek, Z., Lakey, J.H., Macek, P., Menestrina, G., Anderluh, G., 2003. A novel mechanism of pore formation: membrane penetration by the N-terminal amphipathic region of equinatoxin. J. Biol. Chem. 278, 22678–22685. https://doi.org/10.1074/jbc.M300622200.
Mancheño, J.M., Martín-Benito, J., Martínez-Ripoll, M., Gavilanes, J.G., Hermoso, J.A., 2003. Crystal and electron microscopy structures of sticholysin II actinoporin reveal insights into the mechanism of membrane pore formation. Structure 11, 1319–1328. https://doi.org/10.1016/j.str.2003.09.019.
Martinez, D., Campos, A.M., Pazos, F., Alvarez, C., Lanio, M.E., Casallanovo, F., Schreier, S., Salinas, R.K., Vergara, C., Lissi, E., 2001. Properties of St I and St II, two isotoxins isolated from Stichodactyla helianthus: a comparison. Toxicon 39, 1547–1560. https://doi.org/10.1016/S0041-0101(01)00127-1.
Martínez, D., Otero, A., Alvarez, C., Pazos, F., Tejuca, M., Eliana Lanio, M., Gutiérrez-Aguirre, I., Barlic, A., Iloro, I., Luis Arrondo, J., González-Mañas, J.M., Lissi, E., 2007. Effect of sphingomyelin and cholesterol on the interaction of St II with lipidic interfaces. Toxicon 49, 68–81. https://doi.org/10.1016/j.toxicon.2006.09.019.
Maula, T., Isaksson, Y.J.E., García-Linares, S., Niinivehmas, S., Pentikainen, O.T., Kurita, M., Yamaguchi, S., Yamamoto, T., Katsumura, S., Gavilanes, J.G., Martínez-Del-Pozo, Á., Slotte, J.P., 2013. 2NH and 3OH are crucial structural requirements in sphingomyelin for sticholysin II binding and pore formation in bilayer membranes. Biochim. Biophys. Acta Biomembr. 1828, 1390–1395. https://doi.org/10.1016/j.bbamem.2013.01.018.
Michaels, D., 1979. Membrane damage by a toxin from the sea anemone stoichactis helianthus I. Formation of transmembrane channels in lipid bilayers. Biochim. Biophys. Acta 555, 67–78. https://doi.org/10.1016/0005-2736(79)90072-5.
Pedrera, L., Fanani, M.L., Ros, U., Lanio, M.E., Maggio, B., Álvarez, C., 2014. Sticholysin I – membrane interaction: an interplay between the presence of sphingomyelin and membrane fluidity. Biochim. Biophys. Acta Biomembr. 1838, 1752–1759. https://doi.org/10.1016/j.bbamem.2014.03.011.
Pedrera, L., Gomide, A.B., Sánchez, R.E., Ros, U., Wilke, N., Pazos, F., Lanio, M.E., Itri, R., Fanani, M.L., Alvarez, C., 2015. The presence of sterols favors sticholysin I-membrane association and pore formation regardless of their ability to form laterally segregated domains. Langmuir 31, 9911–9923. https://doi.org/10.1021/acs.langmuir.5b01687.
Riske, K., Sudbrack, T., Archilha, N., Uchoa, A., Schroder, A.P., Marques, C., Baptista, M., Itri, R., 2009. Giant vesicles under oxidative stress induced by a membrane-anchored photosensitizer. Biophys. J. 97, 1362–1370. https://doi.org/10.1016/j.bpj.2009.06.023.
Rojko, N., Cronin, B., Danial, J., Baker, M., Anderluh, G., Wallace, M., 2014. Imaging the lipid-phase-dependent pore formation of equinatoxin II in droplet interface bilayers. Biophys. J. 106, 1630–1637. https://doi.org/10.1016/j.bpj.2013.11.4507.
Rojko, N., Dalla, M., Maček, P., Anderluh, G., 2016. Pore formation by actinoporins, cytolysins from sea anemones. Biochim. Biophys. Acta Biomembr. 1858, 446–456. https://doi.org/10.1016/j.bbamem.2015.09.007.
Rojko, N., Kristan, K.C., Viero, G., Zerovnik, E., Macek, P., Dalla Serra, M., Anderluh, G., 2013. Membrane damage by an alpha-helical pore-forming protein, Equinatoxin II, proceeds through a succession of ordered steps. J. Biol. Chem. 288, 23704–23715. https://doi.org/10.1074/jbc.M113.481572.
Ros, U., , Rodr??guez-Vera, W., Pedrera, L., Valiente, P.A., Cabezas, S., Lanio, M.E., , Garc??a-S??ez, A, J., Alvarez, C., 2015. Differences in activity of actinoporins are related with the hydrophobicity of their N-terminus. Biochimie 116, 70–78. https://doi.org/10.1016/j.biochi.2015.06.024.
Rosa, R. De, Spinozzi, F., Itri, R., 2018. Hydroperoxide and carboxyl groups preferential location in oxidized biomembranes experimentally determined by small angle X-ray scattering: implications in membrane structure. Biochim. Biophys. Acta Biomembr. 1860, 2299–2307. https://doi.org/10.1016/j.bbamem.2018.05.011.
Sankhagowit, S., Wu, S., Biswas, R., Riche, C.T., Povinelli, M.L., Malmstadt, N., 2014. The dynamics of giant unilamellar vesicle oxidation probed by morphological transitions. BBA - Biomembr. 1838, 2615–2624. https://doi.org/10.1016/j.bbamem.2014.06.020.
Scanavachi, G., Coutinho, A., Fedorov, A.A., Prieto, M., Melo, A.M., Itri, R., 2021. Lipid hydroperoxide compromises the membrane structure organization and softens bending rigidity. Langmuir 37, 9952–9963. https://doi.org/10.1021/acs.langmuir.1c00830.
Schön, P., García-Sáez, A.J., Malovrh, P., Bacia, K., Anderluh, G., Schwille, P., 2008. Equinatoxin II permeabilizing activity depends on the presence of sphingomyelin and lipid phase coexistence. Biophys. J. 95, 691–698. https://doi.org/10.1529/biophysj.108.129981.
Schrodinger, L., 2018. The PyMOL Molecular Graphics System, Version 2.1.
Siani, P., de Souza, R.M., Dias, L.G., Itri, R., Khandelia, H., 2016. An overview of molecular dynamics simulations of oxidized lipid systems, with a comparison of ELBA and MARTINI force fields for coarse grained lipid simulations. Biochim.

Biophys. Acta Biomembr. 1858, 2498–2511. https://doi.org/10.1016/j.bbamem.2016.03.031.

Soto, C., del Valle, A., Valiente, P.A., Ros, U., Lanio, M.E., Hernández, A.M., Alvarez, C., 2017. Differential binding and activity of the pore-forming toxin sticholysin II in model membranes containing diverse ceramide-derived lipids. Biochimie 138, 20–31. https://doi.org/10.1016/j.biochi.2017.04.003.

Sudbrack, T.P., Archilha, N.L., Itri, R., Riske, K.A., 2011. Observing the solubilization of lipid bilayers by detergents with optical microscopy of GUVs. J. Phys. Chem. B 115, 269–277.

Tanaka, K., Caaveiro, J.M.M., Morante, K., González-Mañas, J.M., Tsumoto, K., 2015. Structural basis for self-assembly of a cytolytic pore lined by protein and lipid. Nat. Commun. 6, 6337. https://doi.org/10.1038/ncomms7337.

Tejuca, M., Dalla Serra, M., Ferreras, M., Lanio, M.E., Menestrina, G., 1996. Mechanism of membrane permeabilization by sticholysin I, a cytolysin isolated from the venom of the sea anemone Stichodactyla helianthus. Biochemistry 35, 14947–14957. https://doi.org/10.1021/bi960787z.

Tejuca, M., Dalla Serra, M., Potrich, C., Alvarez, C., Menestrina, G., 2001. Sizing the radius of the pore formed in erythrocytes and lipid vesicles by the toxin sticholysin I from the sea anemone Stichodactyla helianthus. J. Membr. Biol. 183, 125–135. https://doi.org/10.1007/s00232-001-0060-y.

Tsubone, T.M., Junqueira, H.C., Baptista, M.S., Itri, R., 2019. Contrasting roles of oxidized lipids in modulating membrane microdomains. BBA - Biomembr. 1861, 660–669. https://doi.org/10.1016/j.bbamem.2018.12.017.

Valcarcel, C.A., Dalla Serra, M., Potrich, C., Bernhart, I., Tejuca, M., Martinez, D., Pazos, F., Lanio, M.E., Menestrina, G., 2001. Effects of lipid composition on membrane permeabilization by sticholysin I and II, two cytolysins of the sea anemone Stichodactyla helianthus. Biophys. J. 80, 2761–2774. https://doi.org/10.1016/S0006-3495(01)76244-3.

Veatch, S.L., Keller, S.L., 2003. Separation of liquid phases in giant vesicles of ternary mixtures of phospholipids and cholesterol. Biophys. J. 85, 3074–3083. https://doi.org/10.1016/S0006-3495(03)74726-2.

Weber, G., Charitat, T., Baptista, M., Uchoa, A., Pavani, C., Junqueira, H., Guo, Y., Baulin, V., Itri, R., Marques, C., Schroder, A., 2014. Lipid oxidation induces structural changes in biomimetic membranes. Soft Matter 10, 4241–4247. https://doi.org/10.1039/c3sm52740a.

Wong-Ekkabut, J., Xu, Z., Triampo, W., Tang, I.-M., Tieleman, D.P., Monticelli, L., 2007. Effect of lipid peroxidation on the properties of lipid bilayers: a molecular dynamics study. Biophys. J. 93, 4225–4236. https://doi.org/10.1529/biophysj.107.112565.

Zhao, J., Wu, J., Shao, H., Kong, F., Jain, N., Hunt, G., Feigenson, G., 2007. Phase studies of model biomembranes: macroscopic coexistence of Lalpha+Lbeta, with light-induced coexistence of Lalpha+Lo Phases. Biochim. Biophys. Acta 1768, 2777–2786. https://doi.org/10.1016/j.bbamem.2007.07.009.